Volume 146
Number 4
21 February 2021
Pages 1101-1476

# Analyst

rsc.li/analyst

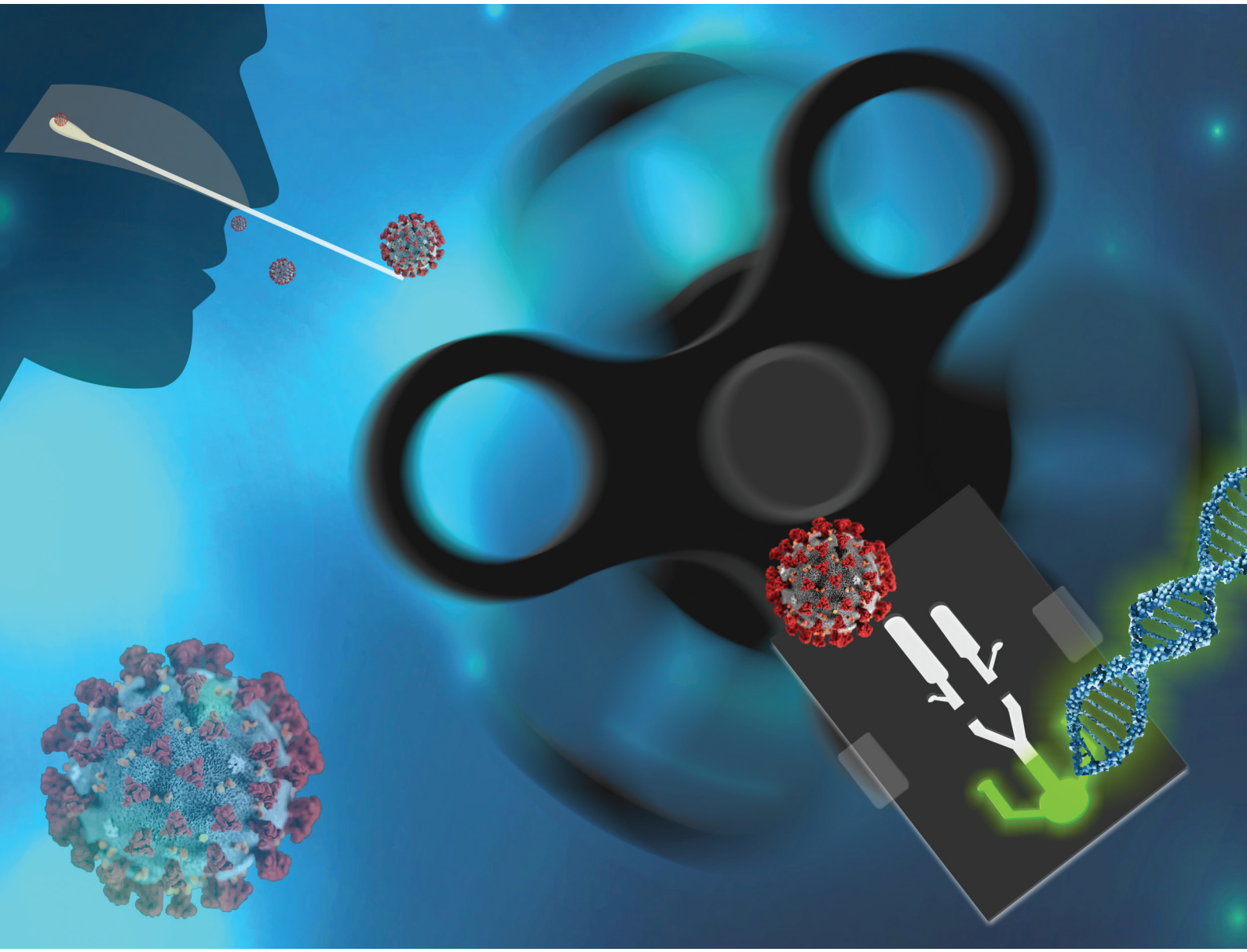

ISSN 0003-2654

ROYAL SOCIETY OF CHEMISTRY

**PAPER**

Gabriela Rodrigues Mendes Duarte *et al.*
Rapid molecular diagnostics of COVID-19 by RT-LAMP in a centrifugal polystyrene-toner based microdevice with end-point visual detection

Analyst

ROYAL SOCIETY OF CHEMISTRY

PAPER

View Article Online
View Journal | View Issue



Cite this: *Analyst*, 2021, **146**, 1178

# Rapid molecular diagnostics of COVID-19 by RT-LAMP in a centrifugal polystyrene-toner based microdevice with end-point visual detection†

Kézia Gomes de Oliveira,‡[a] Paulo Felipe Neves Estrela,‡[a] Geovana de Melo Mendes,‡[a] Carlos Abelardo dos Santos,[b] Elisângela de Paula Silveira-Lacerda [b] and Gabriela Rodrigues Mendes Duarte *[a]

Infection caused by the new coronavirus (SARS-CoV-2) has become a serious worldwide public health problem, and one of the most important strategies for its control is mass testing. Loop-mediated isothermal amplification (LAMP) has emerged as an important alternative to simplify the diagnostics of infectious diseases. In addition, an advantage of LAMP is that it allows for easy reading of the final result through visual detection. However, this step must be performed with caution to avoid contamination and false-positive results. LAMP performed on microfluidic platforms can minimize false-positive results, in addition to having potential for point-of-care applications. Here, we describe a polystyrene-toner (PS-T) centrifugal microfluidic device manually controlled by a fidget spinner for molecular diagnosis of COVID-19 by RT-LAMP, with integrated and automated colorimetric detection. The amplification was carried out in a microchamber with 5 μL capacity, and the reaction was thermally controlled with a thermoblock at 72 °C for 10 min. At the end of the incubation time, the detection of amplified RT-LAMP fragments was performed directly on the chip by automated visual detection. Our results demonstrate that it is possible to detect COVID-19 in reactions initiated with approximately $10^{-3}$ copies of SARS-CoV-2 RNA. Clinical samples were tested using our RT-LAMP protocol as well as by conventional RT-qPCR, demonstrating comparable performance to the CDC SARS-CoV-2 RT-qPCR assay. The methodology described in this study represents a simple, rapid, and accurate method for rapid molecular diagnostics of COVID-19 in a disposable microdevice, ideal for point-of-care testing (POCT) systems.

Received 19th October 2020,
Accepted 2nd January 2021

DOI: 10.1039/d0an02066d

rsc.li/analyst



## 1. Introduction

The new coronavirus pandemic (COVID-19) has already affected 266 countries on all continents, according to the World Health Organization (WHO), causing thousands of deaths.[1] Coronaviruses (order *Nidovirales*, family *Coronaviridae*, subfamily *Coronavirinae*) are a large family of enveloped, positive-sense, single-stranded RNA viruses, with genomes ranging from 26 Kb to 32 Kb.[2] The 2019 novel coronavirus (SARS-CoV-2) was first discovered in the province of Wuhan, China and quickly spread throughout the world. On March 11, 2020, the WHO classified the novel coronavirus disease (COVID-19) outbreak as a pandemic.[1,3] The rapid spread of the ongoing outbreak has become a huge public health issue around the world.[4,5] As with all diseases of great social impact, early and accurate diagnosis of the infection caused by COVID-19 is crucial for the correct treatment of patients and for epidemiological control.[6] The ability to detect an infectious agent quickly in a pandemic is crucial to the success of quarantine efforts, in addition to sensitive and accurate screening for possible cases of infection in patients in a clinical setting.

A rapid and sensitive method of diagnosis that can be carried out from the first day of symptoms is vital to containing a worldwide pandemic.[7] Diagnostic tests based on nucleic acid amplification reactions can achieve high levels of sensitivity and specificity.[8] Real-time reverse transcription PCR (RT-qPCR) is the gold standard for molecular diagnosis of COVID-19.[9] However, the unprecedented demand for PCR reagents around the world, resulting in a bottleneck effect, has substantially reduced the testing capacity of many countries as the number of cases and necessity for testing increase.[10] Furthermore, RT-qPCR is costly and time consuming, and it

[a]*Instituto de Química, Universidade Federal de Goiás, Goiânia-GO 74690-900, Brazil*
[b]*Instituto de Ciências Biológicas, Universidade Federal de Goiás, Goiânia-GO 74690-900, Brazil. E-mail: gabriela_duarte@ufg.br*

†Electronic supplementary information (ESI) available. See DOI: 10.1039/d0an02066d

‡The authors contributed equally to this work.

requires highly trained personnel and expensive laboratory equipment.[11]

Currently, isothermal techniques of nucleic acid amplification have emerged to overcome the limitations of PCR, providing faster and lower cost molecular diagnostics, which can be especially useful for developing countries or in the current situation where the lack of PCR reagents has become an important issue.[12] Loop-mediated isothermal amplification (LAMP) is an amplification technique that does not require heating and cooling cycles; therefore, it requires simpler instrumentation than PCR. LAMP is based on strand displacement activity, which eliminates the need for denaturation of double-stranded DNA. The use of a set of 4–6 specific primers that are able to recognize 6–8 different locations along the target sequence provides LAMP with better specificity than PCR, where the target is recognized in only two locations.[13–15] However, because it is a very powerful amplification technique, a high number of amplicons is produced. For this reason, LAMP manipulation requires extra care to avoid false-positive results. Thus, several studies have reported the importance of performing LAMP in a closed environment, without manipulating the solutions after the reaction has started.[16]

Recently, microfluidic devices built up from different substrates and of diversified fabrication protocols have been widely applied for molecular techniques of diagnosis of COVID-19.[17] Ramachandran and coworkers[18] developed an electrokinetic method in a glass based microfluidic device applicable to CRISPR-based diagnostics with application to detection of SARS-CoV-2 with a total assay time around 30 min with LOD achieved of 10 copies per μL of SARS-CoV-2 RNA. In recent published study, Ji and coworkers[19] developed a complete diagnosis on a microfluidic disc-direct RT-qPCR (dirRT-qPCR). The test was performed within 1.5 hours and detected SARS-CoV-2 with $2 \times 10^1$ copies per reaction. Soares *et al.*[20] developed a cost-effective integrated modular PMMA centrifugal microfluidic platform to perform a 30 min LAMP assay for SARS-CoV-2 detection. The authors reached a limit of detection of $10^2$–$10^3$ copies per reaction.

Microfluidic systems have great potential to automate the manipulation of solutions that support integrated genetic analysis, reducing both the manual contact of the sample and the possibilities of contamination during the analyses.[21] Therefore, microfluidic platforms represent an excellent alternative to LAMP reactions using closed systems since the detection step has the highest risk of contamination, either when removing the solution for gel electrophoresis or when adding the intercalator of DNA for visual detection at the end of the reaction.[22] The integration of steps in microdevices also allows for better manipulation of solutions and a reduction in the total analysis time. In this way, rotationally driven microfluidics offer several advantages for diagnostic testing, facilitating automation and portability of the tests.[23] In general, the operation of the rotating device consists of manipulating it so that as the device is rotated the fluid is pushed in the opposite direction to the center of rotation and can be transported between different chambers through microchannels.[24] The instrumentation used in this type of device can be simplified, and usually the centrifugal pumping is performed using a motor that, through its rotation, moves the fluids in the radial direction, moving it away from the center of rotation.[25] The flow rate of the fluids within the microchannels depends on the speed of rotation, channel size, chamber position, and fluid viscosity.[26] Other functions are possible according to the microfluidic resources used, such as the synchronized release of fluids through the use of valves.[27,28] Ouyang *et al.*[29] described a simple microfabrication method for creating hydrophobic valves using a laser-printed toner in a multilayer polyester-toner (PeT) device. Toner valves have been proven to be effective with aqueous solutions and are easily opened by the application of centrifugal force.

Here, we describe the development of the first polystyrene-toner (PS-T) microfluidic device that is rotationally controlled by a fidget-spinner for molecular diagnosis by RT-LAMP, capable of performing visual detection on-chip by automated mixing of the solution containing the amplicons with the DNA intercalator. The integrated microdevice was used to develop a rapid, sensitive, and straightforward method for molecular diagnosis of COVID-19 by RT-LAMP. The reaction was developed using a simple heating block and on-chip visual detection using SYBR Green I intercalator, aided by a hand-held UV source. Images were obtained with a smartphone.

## 2. Experimental

### 2.1. Virus culture

The virus was cultured in VERO cells, concentrated with $1.6 \times 10^{12}$ PFU $mL^{-1}$ and inactivated. The virus was kindly donated by the Molecular and Clinical Virology Laboratory from University of São Paulo.

### 2.2. Clinical samples

Naso and oropharyngeal swabs were obtained from patients with confirmed COVID-19 during an epidemic in Brazil in April 2020. Confirmation of infection by the COVID-19 virus was obtained from the RT-qPCR results. This study was approved by the Research Ethics Committee of the Federal University of Goias, with protocol number No. 4.111.485. All experiments were performed in compliance with nationally required guidelines, following the resolutions CNS 466/12 and CNS 441/11, and in compliance with institutional guidelines. Furthermore, consent was obtained from all patients. All samples were handled and deactivated first in a biosafety level 2 laboratory with personal protection equipment.

### 2.3. RNA extraction and real-time reverse-transcription PCR

All samples were submitted to RNA extraction using the BioGene® K204 DNA/RNA Extraction kit (produced by Bioclin, Quibasa Química Básica LTDA; ANVISA Registration: 10269360296), following the protocol provided by the manufacturer.

The US CDC SARS-CoV-2 kit was used in the RT-qPCR assays. Briefly, a master mixture was made with 20 μL reaction volume containing 5 μL of RNA template, 13 μL of master mix, 2 μL of primer and probe mix. The PCR mixtures were incubated at 95 °C for 10 min, with 40 cycles of 95 °C for 15 s and 60 °C for 1 min, using the Applied Biosystems Life technologies real-time PCR system. Serial dilution of control plasmids containing the complete nucleocapsid gene from 2019-nCoV (Integrated DNA Technologies, IA, USA) was used to generate a standard curve (SC) for absolute quantification (5 to $2 \times 10^5$ copies of viral RNA) and to obtain cycle threshold (Ct) values. The real-time data was analyzed using the StepOnePlus™ System provided by Applied Biosystems (California, USA).

### 2.4. Fabrication of the PS-T centrifugal microdevice

PS-T microchips were fabricated using a previously described print, cut, and laminate (PCL) protocol.[30] Fig. 1S† shows the main steps of the fabrication process and the top of view of the PS-T centrifugal device. The microchip consisted of four layers of polystyrene films and contain one RT-LAMP chamber of approximately 5 μL (chamber 1), one SYBR Green I (1 : 70) chamber of approximately 3 μL (chamber 2), and one detection chamber, with approximately 8 μL, for mixing solutions after the incubation time. The bottom and top layers of the microdevice were polystyrene films with hydrophobic toner valves (3.3 mm wide) printed at 100% grayscale by laser printing (Brother HL-1212 W) using a black toner cartridge (TN-1060) to define the barriers. The patterned toner was printed on the top and bottom surface. The access holes were pre-cut only on the top sheet. The two intermediated layers were polystyrene sheets covered with toner on both sides using a laser printer (Brother HL-1212 W). The design of the chambers was drawn using Silhouete Studio® software, and the chambers were created by cutting out with a desktop digital craft cutter (Silhouete Cameo, Brazil). The four layers were aligned and laminated together using an office laminator (230c – A4) at 160 °C.

### 2.5. Fidget-spinner to generate the centrifugal force

We utilized a fidget spinner to provide continuous centrifugal force, with just the flick of a finger providing the opening of the valve and the mixture between the amplicons and the SYBR Green I. We spun the fidget spinner by hand and measured the rotation speed with the aid of a cell phone camera. We made videos in slow motion so we could count the number of rotations per minute. We evaluated the use of the fidget spinner by different operators, varying the time from 5–15 s.

### 2.6. Optimization of mixing in the centrifugal microdevice

A preliminary study was carried out to investigate the performance of the fidget spinner to provide a homogeneous mixture in the microdevice, allowing for correct reading of the results. In order to evaluate the efficiency of the mixing in the microdevice, 5 μL of solution from RT-LAMP products that were previously amplified in a tube was added to chamber 1, while 3 μL of SYBR Green I was added to chamber 2. Different mixing protocols were tested by using the fidget spinner until the best condition was found. The mixing efficiency was evaluated by color analysis (bright green fluorescence) of the amplicon solution after mixing with the DNA intercalator (SYBR Green I). The images were obtained with a smartphone and evaluated using ImageJ software. The color intensity was measured using the green channel of the RGB (red, green, blue) color channels. The mixing efficiency was evaluated by calculating the standard deviation of the intensity of green color in different positions of the detection chamber at the end of the mixing steps. A total of five microdevices per spinning test were analyzed. The values were compared with a standard deviation of green color obtained from the premixed reagents (in a tube) introduced into the detection chamber.

### 2.7. RT-LAMP amplification of SARS-CoV-2 in a centrifugal PS-T microdevice

The sequences of primers used for RT-LAMP for SARS-CoV-2 detection, which has been described by Zhang *et al.*,[31] are shown in Table 1.

The main operational steps of the centrifugal RT-LAMP microdevice for SARS-CoV-2 detection are illustrated in Fig. 1.

First, the RT-LAMP master mixture was prepared in a tube and contain: 0.2 μM of each outer primer (F3 and B3), 1.6 μM of each inner primer (FIP and BIP), 0.4 μM of each loop primer (LFP and LBP), 6 mM $MgSO_4$, 1.0 mM dNTP, 0.48 U $\mu L^{-1}$ of *Bst* 3.0 polymerase, 0.5 μL of 10× isothermal amplification buffer [20 mM Tris-HCl, 10 mM KCl, 10 mM $(NH_4)_2SO_4$, 2 mM $MgSO_4$, 0.1% Triton X-100], BSA (0.11 mg $mL^{-1}$), and varying amounts of RNA. Before use, the microchambers were passivated with BSA (5.0 mg $mL^{-1}$), as previously described.[32] Afterwards, 5 μL of the RT-LAMP master mixture was added to the reaction chamber (1), and 3 μL of SYBR Green I (1 : 70) was added to chamber 2. After pipetting the reagents, the top of the microdevice was sealed using clear contact paper to prevent evaporation of the solutions during the incubation time. The microdevice was placed in a thermoblock (Major Science, Saratoga, CA) at 72 °C for 10 min. At the end of the reaction incubation time, the clear contact paper was removed from the top of the microdevice and then the solution with RT-LAMP products was mixed with SYBR Green I for visual detection. For this, the microdevice was rotated using the fidget spinner to generate the centrifugal force necessary to break the hydrophobic valve and to allow the flow of solution in the direction of the detection chamber for visual detection of the amplification products. Then, the detection chamber

**Table 1** Sequences of primers for RT-LAMP

| Primer | 5′ to 3′ |
|---|---|
| F3 | CTGCACCTCATGGTCATGTT |
| B3 | AGCTCGTCGCCTAAGTCAA |
| FIP | GAGGGACAAGGACACCAAGTGTATGGTTGAGCTGGTAGCAGA |
| BIP | CCAGTGGCTTACCGCAAGGTTTTAGATCGGCGCCGTAAC |
| LFP | CCGTACTGAATGCCTTCGAGT |

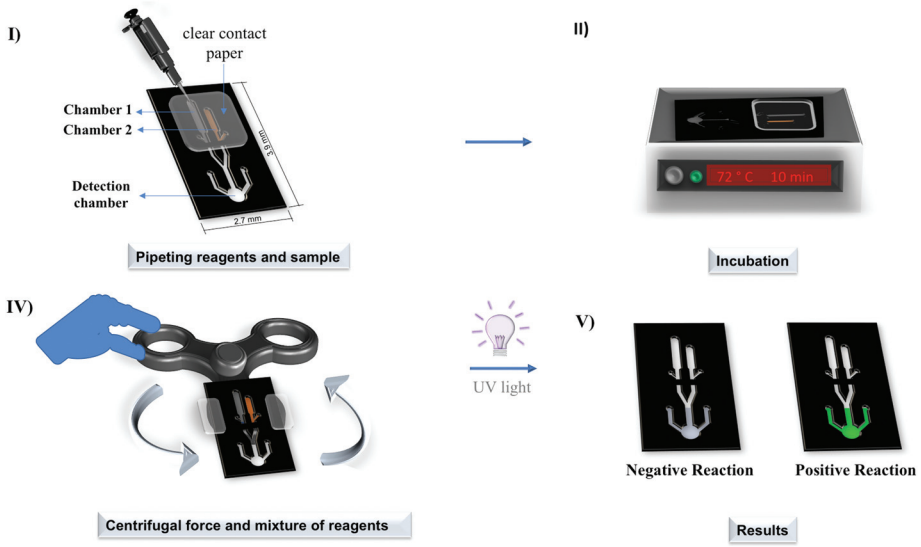


**Fig. 1** Schematic illustration of the RT-LAMP amplification and detection in centrifugal PS-T microdevices: (1) addition of reagents and sealing with clear contact paper; (2) incubation in a thermoblock; (3) centrifugation by fidget spinner for the valve rupture and (4) visual detection by UV radiation.

was exposed to UV light using an UV transilluminator (Hoefer Model: UVIS-20, USA), containing a lamp with a wavelength of 320 nm, and images were taken with a smartphone (MI 8 Lite, M1808D2TG), with the aid of a black acrylic support to control the arbitrary lighting of the room. The support has a cubic format (130 × 100 × 100 $mm^3$) with an opening on top for viewing the chip and accessing the smartphone camera. To demonstrate that the fluorescence was from specific amplification, the solution was removed from the detection chamber for agarose gel electrophoresis.

## 3. Results and discussion

### 3.1. Centrifugal polystyrene-toner microdevice

We previously demonstrated that PeT devices could be successfully used to detect dengue virus (DENV) by amplifying RNA by RT-LAMP.[33] Here, we replaced the previously used polyester films for microdevice fabrication by polystyrene films since these are more transparent to UV radiation at 320 nm than polyester films, as shown in Fig. 2S,† increasing the sensitivity of visual detection. Through the UV-Vis transmittance spectrum (Fig. 2S†), it was observed that polystyrene film shows a significant transmittance spectrum above 290 nm, while polyester transparencies show a significant transmittance spectrum only above 340 nm. Probably the polyester transparency film works as a filter, not allowing UV light to reach the solution effectively, not causing effective excitation and thus reducing the percentage of transmittance in the visible region of the spectrum. Thereby, the spectrum shown in Fig. 2S,† demonstrated that 90.42% of the radiation is transmitted by polystyrene at a wavelength of 320 nm instead of ~50% as the polyester film. In order to provide a better visualization of the fluorescence transmitted directly in the microdevice chamber, and promote an increase in fluorescence emission upon excitation, we have replaced polyester film to polystyrene film. Regarding the performance of the RT-LAMP reaction, the polystyrene film showed the same compatibility with the RT-LAMP reagents as the polyester films. In addition to changing the substrate, here we demonstrated an important advance compared to the previous paper: the integration and automation of visual detection. In our previous paper, although visual detection was done directly on-chip, the addition of the DNA intercalator was carried out after amplification by pipetting SYBR Green I at the end of the reaction incubation time. The integration and automation of visual detection in a closed environment prevents contamination and false-positive results. To allow this integration and automation of mixing RT-LAMP products with SYBR Green I at the end of the incubation time, more functionality was incorporated into the microdevice, such as the hydrophobic valves described by Ouyang *et al.*[29] The hydrophobic valves patterned by laser printer lithography function as a passive valve and provide control of the fluidic manipulation process, driven by a centrifugal force.

We investigated the use of a simple, hand-powered, and electricity-free centrifugal platform based on a commercially available fidget spinner to generate the centrifugal force needed to open the valve and then mixed the RT-LAMP products and SYBR Green I in an automatized manner to visual detection. Most of these commercial fidget spinners contain three wings that present weights that are equally distributed in relation to the center of rotation.[34] Centrifugation is initiated by a hand-generated impulse (external force) on the fidget spinner's wing. This impulse induces the wings to rotate around the central axis through a ball bearing mechanism present in the center of the flat structure. These spheres

reduce friction during rotation, and although the impulse is low, the rotation speed remains high due to the low friction between the outer and inner ring.[35] We measured the rotation speed of the fidget spinner through videos and observed that the speed reached 1200 rpm, varying, on average, from 600 rpm at low speed to 1200 rpm at high speed. The experiments demonstrated that the rotation required to open the hydrophobic valve with 100% gray scale and a width of 3.3 mm was 300 rpm (data not shown); that is, this valve can be easily broken with a fidget spinner. Different rotational forces were used to assess the homogeneity of the mixture in the detection chamber. The homogeneity of the mixture was evaluated through the standard deviation of the green color in the detection chamber. A solution that was considered completely homogeneous was mixed in a tube and then inserted into the detection chamber, obtaining a standard deviation of the color of ~1. Therefore, standard deviations with values close to 1 would correspond to a homogeneous mixture. Fig. 2A shows that the low speed (600 rpm) and high speed (1200 rpm) provide a similar homogenization of the mixture after turning the device twice clockwise (CW) and twice counterclockwise (CCW) with fidget spinner by 5 seconds in each direction. This means that even if the fidget spinner does not have controlled rotation, it is possible to obtain efficient mixing of the solutions, even if different rotations are applied to the fidget spinner.

In order to assess the rotation time in each direction and how many times it would be necessary to produce a homogeneous mixture, a series of experiments were carried out at different times (5–15 s) in alternating directions of rotation (CW and CCW) (Fig. 2B). According to Fig. 2B, the rotation time of 5 s demonstrated the best performance of the reagent mixture, observed by reducing the standard deviation during each direction of rotation. In this way, a homogeneous mixture (standard deviation of 1.35) can be obtained within 5 s in each direction of rotation (totaling 4 rotations CW and 4 rotations CCW), ending the rotation step in ~40 s.

Since it is not possible to manually control the specific speed using the fidget spinner and since it has little dissipative energy force (low friction), the variation in the rotation rate between different operators is common. In this way, centrifugal forces, created by uncontrolled rotations and operated by different users, were also explored in order to demonstrate that even with the existing variations from operator to operator it is possible to arrive at similar final results. To ensure the reproducibility with a different user, we randomly chose three adults (two female and one male) to push the fidget spinner and evaluated the homogeneity of the mixture. According to the data shown in Fig. 2C, even with the variations in the rotation rates from operator to operator, the fluorescence hue showed a uniform distribution as the mixture was rotated

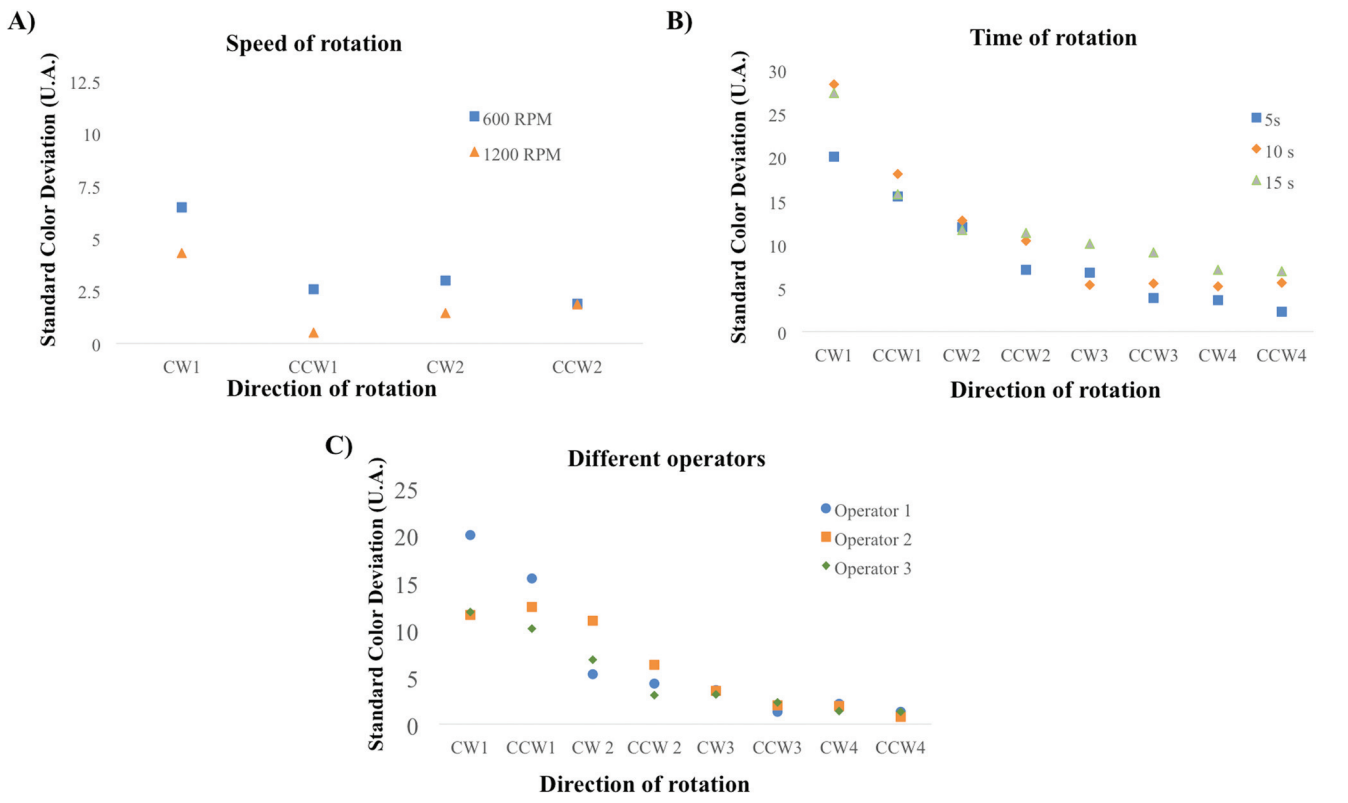


Fig. 2 Evaluation of the homogeneity of the mixture through green color distribution by applying consecutive rotations in different rotational directions (clockwise [CW] and counterclockwise [CCW] rotational movement). (A) Tone standard deviation value at different speeds of rotation, at 600 and 1200 RPM for 5 s in each direction. (B) Evaluation the mixture at different rotation times, 5, 10 and 15 s. (C) Evaluation of the mixture by centrifugal pumping *via* fidget-spinner, without control of the rotation rate, using 3 different operators.

alternately CW and CCW. The uniform distribution was found for the three operators in the fourth rotation cycle through the values of the standard deviations of 1.31, 0.73, and 1.32 for operators 1, 2, and 3, respectively. Thus, even at different speeds of rotation, it is possible to obtain similar results of homogeneity of the mixture, proving that the test can be performed regardless of the operator.

### 3.2. RT-LAMP

For SARS-CoV-2 in the PS-T centrifugal microdevice, we initially optimized the composition of the master mixture. The concentrations of enzyme, primers, and dNTP were optimized. As demonstrated in previous studies,[33] the LAMP performed on microfluidic devices requires a higher concentration of enzyme due to the large area/volume ratio of the reaction chamber. In this study, we observed that the minimum enzyme concentration for success of the reaction was 0.48 U $\mu L^{-1}$, and this concentration was sufficient for the success of the reaction even with low RNA copies. The optimized concentrations of dNTPs and primers that demonstrated better RT-LAMP efficiency and prevented false-positive results were 1.0 mM of dNTP and 0.2 μM of each outer primer (F3 and B3), 1.6 μM of each inner primer (FIP and BIP), and 0.4 μM of each loop primer (LFP and LBP).

In order to obtain a rapid test for the diagnosis of COVID-19, maintaining high sensitivity, the incubation time was optimized by testing 5, 10, 15, 20, and 30 min of heating at 72 °C. The results of the optimization of the incubation time showed that 10 min was the shortest time that produced detectable quantities of fragments in the visual detection and in the agarose gel (Fig. 3B). False-positive results were observed with incubation times greater than 20 min (Fig. 3A). Therefore, all assays were carried out using 10 min of incubation time.

Until today, for SARS-CoV-2 detection by RT-LAMP in microtubes the optimum time of the reaction ranged from 30 min to 60 min[17,24,31,36,37] In most of these papers the authors used the *Bst* 2.0 version, and this explains the longer time of RT-LAMP. In our previous study, we demonstrated that the *Bst* 2.0 needs longer heating time than *Bst* 3.0.[33] In addition, use of the enzyme *Bst* 3.0 lowers the cost of the reaction since it does not require the use of an extra transcriptase enzyme, and it provides results in shorter analysis times. Since *Bst* 3.0 provides the fastest amplification time, it is an ideal candidate for use in methods for the rapid diagnosis of COVID-19.

### 3.3. Sensitivity

The analytical sensitivity (limit of detection) of RT-LAMP in a centrifugal PS-T was determined by serial dilution of RNA from SARS-CoV-2. Reactions were performed with initial amounts of RNA ranging from $10^{7}$ to $10^{-6}$ copies of RNA. The centrifugal PS-T platform allowed for detection of amplicons on the agarose gel in reactions starting with as low as $10^{-4}$ copies per microliter of viral genome copies (Fig. 4S†).

A great advantage of the LAMP reaction is the possibility of performing visual detection without the need for electrophoresis, allowing for easy and quick reading of the results. The use of DNA intercalating reagents as a strategy for detection LAMP, due to the methodological convenience, is already well explored in the literature.[38–40] The fluorescence intensity for positive reactions varies according to the initial RNA copy number, as can be seen in Fig. 4A. We show here that analysis of the intensity of the green color in the detection chamber can be used for reasonable quantification of the viral load. The images were obtained with a cell phone camera and evaluated using the ImageJ program. The intensity of color was measured using the green channel of the RGB (red, green,

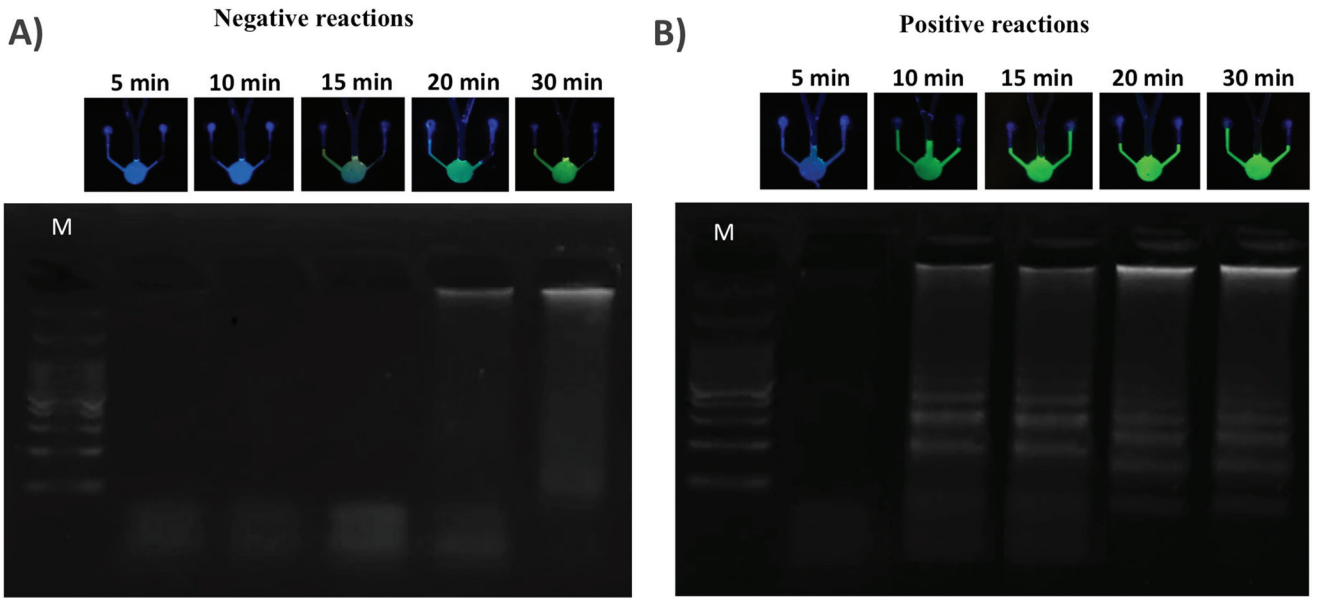


**Fig. 3** Evaluation of incubation time of RT-LAMP in centrifugal microdevice. In panels A: NTC (non-template control) reactions and B: positive control reactions. In both panels: M: molecular weight marker.

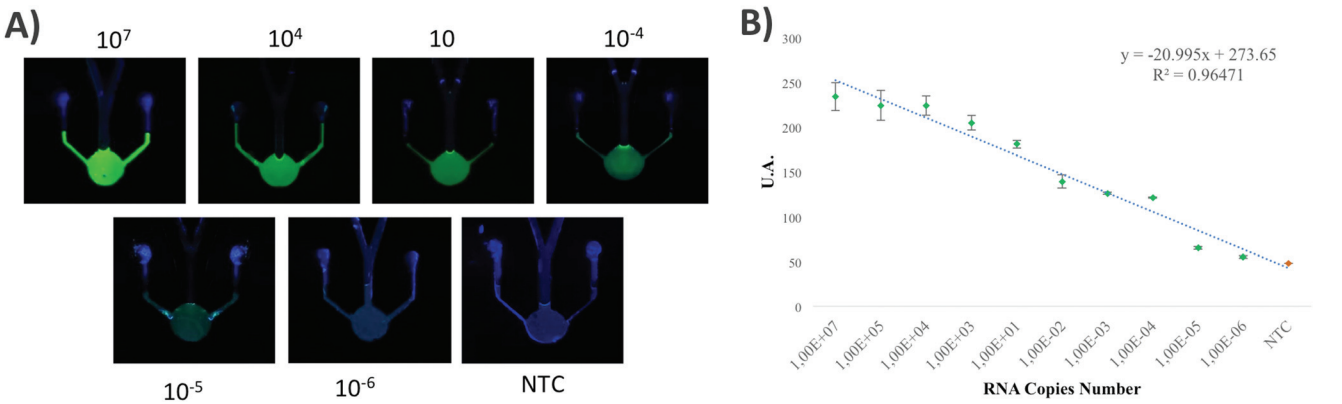


Fig. 4 Visual detection of SARS-CoV-2 amplification products *via* RT-LAMP in different amounts of initial copies of the target ($10^7$–$10^{-6}$ DNA copy). (A) Visual detection; (B) digital analysis of the images of the reactions performed in triplicate, by the ImageJ software for quantitative correlation with the intensity of the fluorescence. NTC, no template control.



blue) color channels. Fig. 4B shows the reasonable linear behavior, with $R^2$ = 0.9647, of the logarithm of fluorescence intensity *versus* the number of initial copies of RNA. The RSD values ($n$ = 3) were calculated and ranged from 0.017 to 6.69%. Considering the image capture through a cell phone, the RSD values were satisfactory, thus revealing a good potential for reasonable quantification of the viral load involving real samples.

The visual assessment of the shade of green and the analysis of the intensity of green in the RGB channel were in agreement to electrophoresis gel (Fig. 4S†). These results coincide with the results shown by the electrophoretic separation in the agarose gel.

Considering 8 independent replicates for each RNA concentration, the probit regression analysis revealed that the limit of detection at 95% probability was $-2.91 \log_{10}$ ($\sim 1.0 \times 10^{-3}$) copies of SARS-CoV-2 RNA, with confidence interval from −3.58 to −1.29 (Table 2 and Fig. 3S†).

This low limit of detection of RT-LAMP means that the technique is able to detect the presence of SARS-CoV-2, even in patients with low viral loads, thus allowing for early diagnosis of COVID-19.

Currently, some studies have reported the molecular detection of SARS-CoV-2 by LAMP in tubes with a limit of detection of 0.1–10 copies per μL.[41,42] A recently published study by Soares *et al.*[20] reported a LAMP assay performed on a PMMA-based microfluidic platform with a detection limit of $10^2$–$10^3$ copies per reaction and an analysis time of 30 min. Rodriguez-Manzano and coworkers[43] described a LAMP assay in a cartridge microfluidic device for the detection of SARS-CoV-2 RNA samples showing a limit of detection of 10 RNA copies per reaction in under 20 minutes. In a study reported by Tian *et al.*[44] a fully automated centrifugal microfluidic system was used to detect SARS-CoV-2 through a 70 min RT-LAMP assay with a limit of detection of 2 copies per reaction. The limit of detection found in this present study is lower than those reported in the literature, which has great potential for diagnosing COVID-19, even in the beginning of the infection. In a study of samples collected during the clinical course of COVID-19, Wölfel *et al.*[45] demonstrated a high viral load at the onset of symptoms (the mean RNA load of the virus was $6.76 \times 10^5$ copies per swab for up to 5 days). Considering that the value is substantially higher than the limit of detection obtained in this study, our methodology presents the possibility of detecting the virus from the first days of infection. The limit of detection of $-2.91 \log_{10}$ ($\sim 10^{-3}$) RNA copies found here for SARS-CoV-2 detection was similar to the limit of detection found in our previous study for Zika virus detection using *Bst* 3.0 with 10 min of reaction.[46] Due to the impressively low detection limit, our methodology and platform were proven to be an important tool that can be used in samples collected immediately after the onset of symptoms, allowing diagnosis in the early stages of infection when the detection of antibodies is still negative.

Table 2 Limit of detection (LOD) of the SARS-CoV-2 RT-LAMP assay. Probit regression analysis was calculated using MedCalc software (version 18.11), giving a C95 value (concentration detectable 95% of the time) of $-2.91 \log_{10}$ of initial copies of SARS-CoV-2

| SARS-CoV-2 concentration (initial copies) | No. of replicates | No. of positive results | Hit rate in % |
|---|---|---|---|
| $1.0 \times 100$ | 8 | 8 | 100 |
| $1.0 \times 10^{-2}$ | 8 | 8 | 100 |
| $1.0 \times 10^{-3}$ | 8 | 7 | 87.5 |
| $1.0 \times 10^{-4}$ | 8 | 6 | 75 |
| $1.0 \times 10^{-5}$ | 8 | 3 | 37.5 |
| $1.0 \times 10^{-6}$ | 8 | 0 | 0 |
| $1.0 \times 10^{-7}$ | 8 | 0 | 0 |

### 3.4. Evaluation of RT-LAMP in a centrifugal PS-T microdevice assay in clinical samples

We evaluated the performance of the PS-T centrifugal microdevice for diagnosing COVID-19 in real clinical samples. As a proof-of-concept of the capability of our platform in the diagnosis of COVID-19, we used 20 real samples previously tested by RT-qPCR. Of these 20 samples, ten were negative and ten tested positives by RT-LAMP. The samples confirmed a 100%

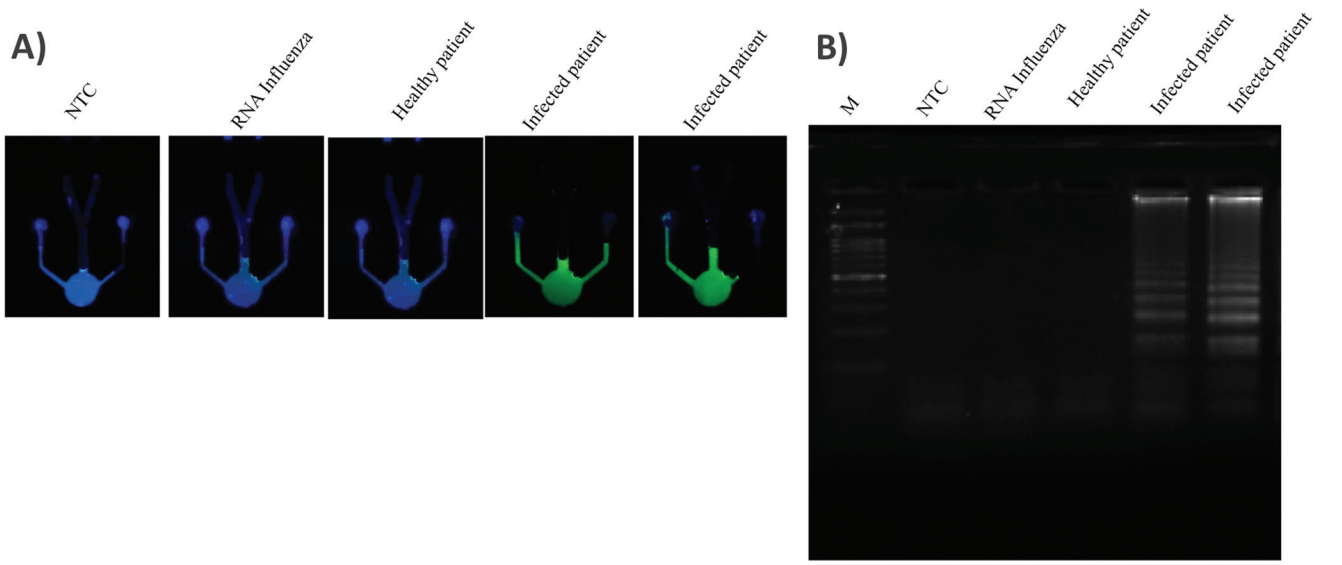


**Fig. 5** Evaluation of specificity and clinical samples analysis by RT-LAMP for detection of SARS-CoV-2. (A) Visual detection on-chip. (B) Detection off-chip: agarose gel.

agreement between the RT-LAMP-based test carried out in this study in the PS-T centrifugal device (with 10 min of reaction) with qPCR assays, which is considered the gold standard for the molecular diagnosis of COVID-19.

The specificity of the RT-LAMP primers used in this study for detection of SARS-CoV-2 was demonstrated by using influenza virus samples from healthy patients and samples from patients infected with SARS-CoV-2. We found that fluorescence increased when SARS-CoV-2 was used as the template and not with other virus samples or healthy human samples (Fig. 5), demonstrating the high level of RT-LAMP specificity. Fig. 5S† shows the visual detection from the 20 real clinical samples (10 positives and 10 negatives).

These preliminary results revealed that the proposed RT-LAMP in a centrifugal PS-T microdevice assay had a high sensitivity and specificity for diagnosis of COVID-19, in addition to the great potential for applications in point-of-care.

## 4. Conclusion

We report a 10 min assay for the detection of SARS-CoV-2 based on a RT-LAMP reaction carried out in a disposable centrifugal microdevice. The integration and automation of the RT-LAMP reaction with visual detection in the centrifugal device allows the entire process to be carried out in a closed environment, thus avoiding contamination and false-positive results. In addition, the advantage of integrated and automated visual detection provided by a hand-powered, electricity-free centrifugation platform using a fidget spinner is to obtain fast results, eliminating pipetting steps.

In the tests carried out in the PS-T microchip, it was possible to detect amplicons in reactions that started with $-2.91 \log_{10}$ ($\sim 10^{-3}$) copies of SARS-CoV-2 RNA with on-chip detection. This detection limit is significantly lower than recent published studies describing LAMP in microdevices for the diagnosis of COVID-19.[20,43,44]

The low detection limit found in this study is due to the fact that the use of SYBR Green leads to increased sensitivity when compared with others detection method.[47] However, the inhibitory effect of SYBR Green on the LAMP reaction is well established.[48] For this reason, the intercalating dye addition step at the end of the reaction is necessary. In this paper, the microchip developed allowed the integration of this step, representing advances in relation to previous studies.[32,33] However, the demand for extraction off-chip are still limitations to be overcome for the obtainment a fully integrated microchip for molecular diagnostic.

It is also important to consider the cost of our test, which is much less than the cost of a test based on qPCR. While a diagnosis involving the qPCR methodology costs, on average, ~US $100.00 per test, the diagnosis using our methodology and our device costs less than US $5.00 (including microchips and reagents).

The RT-LAMP based tests carried out in a disposable and low-cost microdevice represents the first step in the application of molecular diagnostics for point-of-care tests. The entire system can be miniaturized to have a specific and simple molecular diagnosis that can be taken to a remote location. Due to its simple operation and lack of sophisticated instrumentation, the RT-LAMP performed in the PS-T centrifugal platform has proven to be a valuable tool for molecular diagnosis of COVID-19, especially in resource-limited regions of the world.

## Conflicts of interest

There are no conflicts to declare.

## Acknowledgements

We are grateful to Molecular and Clinical Virology Laboratory from University of São Paulo, who kindly donated the inactivated SARS-CoV-2 virus culture. This study was supported by the Labor Prosecution Service, CNPq (grant numbers: 402694/2020-1), FAPEG (grant numbers: 202010267000273), and FINEP (01.16.0049.02 (0247/16).

## References

1 WHO, *World Heal. Organ*, 2020, vol. 2019, p. 2633.
2 M. F. Chiari, *Tese Mestr*, Univ Federal São Carlos, 2010.
3 C. Sohrabi, Z. Alsafi, N. O'Neill, M. Khan, A. Kerwan, A. Al-Jabir, C. Iosifidis and R. Agha, *Int. J. Surg.*, 2020, **76**, 71–76.
4 F. Jiang, L. Deng, L. Zhang, Y. Cai, C. W. Cheung and Z. Xia, *J. Gen. Int. Med.*, 2020, **35**, 1545–1549.
5 C. Wang, P. W. Horby, F. G. Hayden and G. F. Gao, *Lancet*, 2020, **395**, 470–473.
6 D. K. W. Chu, Y. Pan, S. M. S. Cheng, K. P. Y. Hui, P. Krishnan, Y. Liu, D. Y. M. Ng, C. K. C. Wan, P. Yang, Q. Wang, M. Peiris and L. L. M. Poon, *Clin. Chem.*, 2020, **66**, 549–555.
7 L. L. M. Poon, K. H. Chan, O. K. Wong, W. C. Yam, K. Y. Yuen, Y. Guan, Y. M. D. Lo and J. S. M. Peiris, *J. Clin. Virol.*, 2003, **28**, 233–238.
8 H. Zhu, Z. Fohlerová, J. Pekárek, E. Basova and P. Neužil, *Biosens. Bioelectron.*, 2020, **153**, 112041.
9 V. M. Corman, O. Landt, M. Kaiser, R. Molenkamp, A. Meijer, D. K. W. Chu, T. Bleicker, S. Brünink, J. Schneider, M. L. Schmidt, D. G. Mulders, B. L. Haagmans, B. Van Der Veer, S. Van Den Brink, L. Wijsman, G. Goderski, J. L. Romette, J. Ellis, M. Zambon, M. Peiris, H. Goossens, C. Reusken, M. P. G. Koopmans and C. Drosten, *Eurosurveillance*, 2020, **25**, 1–8.
10 I. Yelin, N. Aharony, E. S. Tamar, A. Argoetti, E. Messer, D. Berenbaum, E. Shafran, A. Kuzli, N. Gandali, T. Hashimshony, Y. Mandel-Gutfrend, M. Halberthal, Y. Geffen, M. Szwarcwort-Cohen and R. Kishony, *Clin. Infect. Dis.*, 2020, **71**, 2073–2078.
11 X. Zhu, X. Wang, L. Han, T. Chen, L. Wang, H. Li, S. Li, L. He, X. Fu, S. Chen, M. Xing, H. Chen and Y. Wang, *Biosens. Bioelectron.*, 2020, DOI: 10.1016/j.bios.2020.112437.
12 B. Udugama, P. Kadhiresan, H. N. Kozlowski, A. Malekjahani, M. Osborne, V. Y. C. Li, H. Chen, S. Mubareka, J. Gubbay and W. C. W. Chan, *ACS Nano*, 2020, **14**, 3822–3835.
13 T. Notomi, H. Okayama, H. Masubuchi, T. Yonekawa, K. Watanabe, N. Amino and T. Hase, *Nucleic Acids Res.*, 2000, **28**, e63.
14 Y. Mori and T. Notomi, *J. Infect. Chemother.*, 2009, **15**, 62–69.
15 M. Parida, S. Sannarangaiah, P. K. Dash, P. V. L. Rao and K. Morita, *Rev. Med. Virol.*, 2009, **19**, 57–64.
16 E. J. Kil, S. Kim, Y. J. Lee, E. H. Kang, M. Lee, S. H. Cho, M. K. Kim, K. Y. Lee, N. Y. Heo, H. S. Choi, S. T. Kwon and S. Lee, *J. Virol. Methods*, 2015, **213**, 68–74.
17 H. Zhu, H. Zhang, S. Ni, M. Korabečná, L. Yobas and P. Neuzil, *TrAC, Trends Anal. Chem.*, 2020, **130**, DOI: 10.1016/j.trac.2020.115984.
18 A. Ramachandran, D. A. Huyke, E. Sharma, M. K. Sahoo, C. Huang, N. Banaei, B. A. Pinsky and J. G. Santiago, *Proc. Natl. Acad. Sci. U. S. A.*, 2020, 29518–29525.
19 M. Ji, Y. Xia, J. F. C. Loo, L. Li, H. P. Ho, J. He and D. Gu, *RSC Adv.*, 2020, **10**, 34088–34098.
20 R. R. G. Soares, A. S. Akhtar, I. F. Pinto, N. Lapins, D. Barrett, G. Sandh, X. Yin, V. Pelechano and A. Russom, *medRxiv*, 2020, DOI: 10.1101/2020.11.04.20225888.
21 Y. Yang, Y. Chen, H. Tang, N. Zong and X. Jiang, *Small Methods*, 2020, **4**, 1–30.
22 E. F. M. Gabriel, B. G. Lucca, G. R. M. Duarte and W. K. T. Coltro, *Anal. Methods*, 2018, **10**, 2952–2962.
23 B. S. Lee, Y. U. Lee, H. S. Kim, T. H. Kim, J. Park, J. G. Lee, J. Kim, H. Kim, W. G. Lee and Y. K. Cho, *Lab Chip*, 2011, **11**, 70–78.
24 G.-S. Park, K. Ku, S.-H. Baek, S.-J. Kim, S. Il Kim, B.-T. Kim and J.-S. Maeng, *J. Mol. Diagn.*, 2020, 1–8.
25 K. R. Jackson, J. C. Borba, M. Meija, D. L. Mills, D. M. Haverstick, K. E. Olson, R. Aranda, G. T. Garner, E. Carrilho and J. P. Landers, *Anal. Chim. Acta*, 2016, **937**, 1–10.
26 Y. Ren and W. W. F. Leung, *Chem. Eng. J.*, 2013, **215–216**, 561–578.
27 J. A. Duvall, D. Le Roux, A. C. Tsuei, B. L. Thompson, C. Birch, J. Li, D. A. Nelson, D. L. Mills, M. M. Ewing, R. S. McLaren, D. R. Storts, B. E. Root and J. P. Landers, *Anal. Methods*, 2016, **8**, 7331–7340.
28 T. H. G. Thio, S. Soroori, F. Ibrahim, W. Al-Faqheri, N. Soin, L. Kulinsky and M. Madou, *Med. Biol. Eng. Comput.*, 2013, **51**, 525–535.
29 Y. Ouyang, S. Wang, J. Li, P. S. Riehl, M. Begley and J. P. Landers, *Lab Chip*, 2013, **13**, 1762–1771.
30 B. L. Thompson, Y. Ouyang, G. R. M. Duarte, E. Carrilho, S. T. Krauss and J. P. Landers, *Nat. Protoc.*, 2015, **10**, 875–886.
31 Y. Zhang, N. Odiwuor, J. Xiong, L. Sun, R. O. Nyaruaba, H. Wei and N. A. Tanner, *medRxiv*, 2020, **2**, DOI: 10.1101/2020.02.26.20028373.
32 K. G. de Oliveira, J. C. Borba, A. M. Bailão, C. M. de Almeida Soares, E. Carrilho and G. R. M. Duarte, *Anal. Biochem.*, 2017, **534**, 70–77.
33 G. M. Mendes, K. G. Oliveira, J. C. Borba, T. S. Oliveira, F. S. Fiaccadori, M. L. Nogueira, A. M. Bailão, C. M. A. Soares, E. Carrilho and G. R. M. Duarte, *J. Braz. Chem. Soc.*, 2019, **30**, 1841–1849.
34 J. Koo and D. Y. Tamura, *Clin. Pediatr.*, 2018, **57**, 857–860.
35 E. J. Cohen, R. Bravi and D. Minciacchi, *Sci. Rep.*, 2018, **8**, 1–9.
36 M. Jiang, W. Pan, A. Arastehfar, W. Fang, L. Ling, H. Fang, F. Farnaz Daneshnia, J. Yu, W. Liao, H. Pei, X. Li and C. Lass-Florl, *medRxiv*, 2020, 20036376.

 

37 L. E. Lamb, S. N. Bartolone, E. Ward and M. B. Chancellor, *Lancet*, 2020, DOI: 10.1371/journal.pone.0234682.
38 I. P. Oscorbin, E. A. Belousova, A. I. Zakabunin, U. A. Boyarskikh and M. L. Filipenko, *BioTechniques*, 2016, **61**, 20–25.
39 M. M. Parida, S. Sannarangaiah, P. K. Dash, P. V. L. Rao and K. Morita, *Rev. Med. Virol.*, 2008, **18**, 407–421.
40 Y. P. Wong, S. Othman, Y. L. Lau, S. Radu and H. Y. Chee, *J. Appl. Microbiol.*, 2018, **124**, 626–643.
41 M. El-Tholoth, H. H. Bau and J. Song, *ChemRxiv*, DOI: 10.26434/chemrxiv.11860137.
42 R. Lu, X. Wu, Z. Wan, Y. Li, L. Zuo, J. Qin, X. Jin and C. Zhang, *Virol. Sin.*, 2020, **35**, DOI: 10.1007/s12250-020-00218-1.
43 J. Rodriguez-Manzano, K. Malpartida-Cardenas, N. Moser, I. Pennisi, M. Cavuto, L. Miglietta, A. Moniri, R. Penn, P. Randell, G. Satta, F. Davies, F. Bolt, W. Barclay, A. Holmes and P. Georgiou, *medRxiv*, 2020, DOI: 10.21428/2e3983f5.d2f6c87c.
44 F. Tian, C. Liu, J. Deng, Z. Han, L. Zhang, Q. Chen and J. Sun, *Sci. China: Chem.*, 2020, **63**, 1498–1506.
45 R. Wölfel, V. M. Corman, W. Guggemos, M. Seilmaier, S. Zange, M. A. Müller, D. Niemeyer, T. C. Jones, P. Vollmar, C. Rothe, M. Hoelscher, T. Bleicker, S. Brünink, J. Schneider, R. Ehmann, K. Zwirglmaier, C. Drosten and C. Wendtner, *Nature*, 2020, **581**, 465–469.
46 P. F. N. Estrela, G. de M. Mendes, K. G. de Oliveira, A. M. Bailão, C. M. de A. Soares, N. A. Assunção and G. R. M. Duarte, *J. Virol. Methods*, 2019, **271**, 113675.
47 X. Zhang, S. B. Lowe and J. J. Gooding, *Biosens. Bioelectron.*, 2014, **61**, 491–499.
48 T. L. Quyen, T. A. Ngo, D. D. Bang, M. Madsen and A. Wolff, *Front. Microbiol.*, 2019, **10**, 1–12.